Accepted for presentation at the 29th International Symposium on Shock Waves. Madison, WI. July 14-19, 2013. Paper #0280

Geometric Acoustics in High-Speed Boundary Layers

N. J. Parziale, J. E. Shepherd, and H. G. Hornung

1 Introduction

A key mechanism responsible for the instability of high-speed boundary layers are the high-frequency modes discovered by Mack [1]. These modes are primarily acoustic in nature, are always present if the edge Mach number is sufficiently large, and are the dominant instability mechanism when the wall temperature is sufficiently low compared to the recovery temperature. The propagation of acoustic waves within the boundary layer is profoundly influenced by the velocity and sound speed gradients created by the action of viscosity and heat conduction within the layer. These gradients form a waveguide that may trap acoustic waves and provide a mechanism for the formation of large amplitude disturbances. This suggests that geometrical acoustic analysis of these waveguides can provide insights into the potential for boundary layer acoustic instability. In this work, we outline the basics of geometric acoustics, apply the ray-tracing technique to example problems, and then high-speed boundary layers. The refractive behavior of different high-speed boundary layer profiles is compared.

Our approach follows the classical ray-tracing approach [2, 3] to geometrical acoustics in which the propagation of a wavefront is calculated by computing the paths (rays) along which a point on the wavefront moves. From a physical point of view, geometrical acoustics is a high-frequency approximation that is valid when: 1) the wavelengths are small compared to the geometrical features in the flow, in this case the height of the boundary layer; 2) the amplitude and front curvature do not vary too rapidly along the wavefront; 3) cusps or folds (caustics) do not form in the wavefront. In high-speed boundary layer profiles, the most amplified acoustic wavelength is known to be approximately 2 boundary layer thicknesses [1] and caustics are known to form [4] so we acknowledge from the outset that our

GALCIT, California Insitute of Technology
1200 E California Blvd; MC 205 45, Pasadena, CA 91125, United States of America

results may be limited in quantitative applicability and will be more qualitative in nature.

The rate of change of the position of a point x_p on the wave-front can be written as,

$$\frac{dx_{pi}}{dt} = n_i c + v_i = v_{ray,i} \tag{1}$$

where v_i is the local velocity, n_i is the unit normal to the wave-front τ_i (Fig. 1). The speed of the wave-front normal to itself ($c + n_i v_i$) is in general different than the magnitude of the ray velocity $|n_i c + v_i|$. The evolution of the unit normal n_i is

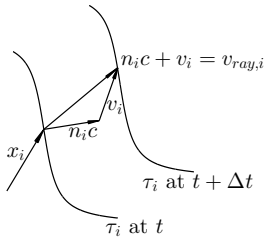

Fig. 1 Vector addition to find the velocity of the rays.

cumbersome to compute directly so we use the formulation by Pierce [2] in terms of the wave-slowness vector ($s_i = \bigtriangledown \tau_i$) components.

$$\frac{dx_i}{dt} = \frac{c^2 s_i}{\Omega} + v_i, \tag{2a}$$

$$\frac{ds_i}{dt} = -\frac{\Omega}{c}\frac{dc}{dx_i} - \sum_{j=1}^{3} s_j \frac{dv_j}{dx_i}, \tag{2b}$$

where,

$$\Omega = 1 - v_i s_i, \tag{3a}$$

$$s_i = \frac{n_i}{c + n_i v_i}. \tag{3b}$$

2 Example Problems

Solutions to two example problems are presented here to provide basic insight into geometric acoustics as well as test our numerical methods. The first test problem is an adaptation from the work of Goodman and Duykers [5]. Analytic solutions for ray paths are found for a parabolic sound speed profile of the form $c = c_0 + \alpha^2 y^2$, with $1/c^2 = (1/c_0^2)(1 - y^2/L^2)$, and $L = \sqrt{c_0/2\alpha^2}$. In the example presented here, $c_0 = 340$ m/s, $\alpha = \sqrt{c_0/10}$, and a rigid boundary at $y = 0$ is imposed. The solution

for a ray path with initial angle of inclination to the horizontal θ_0, is

$$y/L = \sin\theta_0 \sin\left(x/(L\cos\theta_0)\right). \tag{4}$$

This solution (solid line) and results from numerically integrating Eqs. 2 (circular markers) are shown to agree favorably in Fig. 2. In this scenario, s_x is a constant, per Eq. 2b. To calculate the point at which acoustic rays are refracted back to the surface, it is recognized that the ray direction is parallel to the unit normal, n, when horizontal [2], and from Eq 3b,

$$s_x = \frac{\cos\theta_0}{c_0 + \cos\theta_0 v_{x0}} = c_h + v_{xh}, \tag{5}$$

where the subscript 0 indicates where local value at ray origin, and the subscript h indicates local value where the ray is horizontal. Using this observation, the wall normal distance where the ray is refracted back to the surface can be obtained algebraically. The predicted height (dashed line) shows favorable agreement with the analytic and numerical results in Fig. 2. Note the acoustic rays are refracted towards a sound speed minimum, consistent with the vertical component of Eq. 2b.

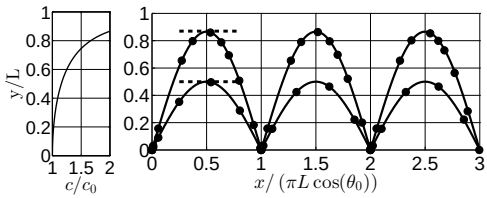

Fig. 2 A slight modification to the problem posed by Goodman and Duykers [5], with the analytical solution (solid line), numerical integration (circular markers), and predicted turning height (dashed line) showing good agreement. Initial angle of inclination of acoustic ray to the surface: $\theta_0 = 30, 60$. The sound speed profile is plotted on the left.

The second test problem is ray tracing through the Sound Fixing and Ranging (SOFAR) channel as previously computed by Munk [6], who assumed that the sound speed in the ocean, c, varies as $c = c(y) = c_1(1 + \varepsilon(\eta(y) + e^{-\eta(y)} - 1))$, due to temperature and density gradients, where $c_1 = 1.492$ km/s, $\varepsilon = 0.0074$, $\eta = \eta(y) = (z - z_1)/(z_1/2)$, and $z_1 = 1.3$ km. Numerical integration of Eqs. 2 with this sound speed profile gives reasonable visual agreement with Munk's results, although precise quantitative comparison is not possible. Acoustic rays are observed to be refracted to a sound speed minimum, which is consistent with Eq. 2b.

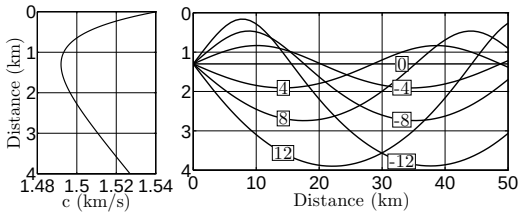

Fig. 3 Replication of the case done by Munk [6], tracing acoustic rays through the SOFAR channel. The distance marks depth from the ocean surface, and the initial angle of the ray to the horizontal is denoted by a number overlaid on the line.

3 High-speed Boundary Layers

Geometrical acoustic implications for a selection of high-speed boundary layer profiles are presented in this section. Boundary layer profiles are computed using the similarity solution for a laminar, compressible, perfect-gas flow on a flat plate [7]. It was noted in the previous section that acoustic rays tend to be refracted towards sound speed minima. The mean flow of the boundary layer modifies this and the rays are refracted toward $u+c$ minima, consistent with the vertical component of Eq. 2b. Three different profiles are presented in Figs. 4(a), 4(b), and 4(c) to illustrate the range of $u+c$ profiles that are possible.

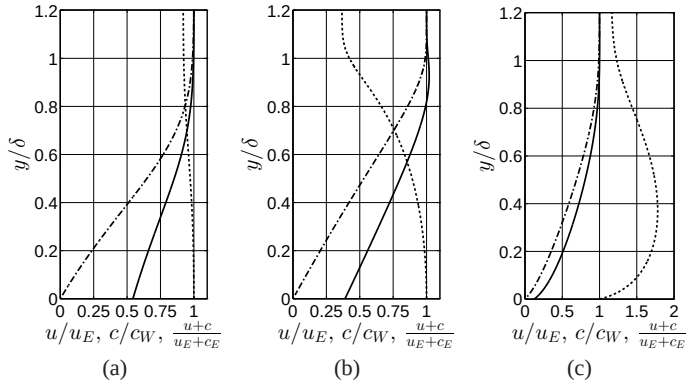

Fig. 4 a: Boundary layer profile for $M_E = 1$, $\gamma = 7/5$, $T_W = T_{ad}$. b: Boundary layer profile for $M_E = 6$, $\gamma = 7/5$, $T_W = T_{ad}$. c: Boundary layer profile for $M_E = 6$, $\gamma = 7/5$, $T_W = T_{ad}/10$. Each velocity profile (u/u_E) is normalized by the edge value (dash-dot). Each sound speed profile c/c_W is normalized by the value at the wall (dashed). Each combined profile $(u+c)/(u_E+c_E)$ is normalized by the edge values (solid).

Using Eq. 5 and assuming that the flow is locally parallel, the maximum angle that is refracted back to the surface can be found. We postulate that the larger this angle, the more unstable the boundary layer due to the larger amount of acous-

tic energy trapped within the layer. The maximum angle of inclination is computed for rays originating at the surface of the plate for a range of Mach numbers ($M_E = 0.25 - 8$) with an adiabatic wall and three different ratios of specific heats in Fig. 5(a). The maximum angle increases with increasing Mach number, reaching a constant value for $M_E \geq 5$. Wall temperature ratio (T_W/T_{ad}, where T_{ad} is the adiabatic wall temperature) is another important parameter in determining the maximum initial angle of inclination for rays originating at the surface of the plate (Fig. 5(b)); at $M_E = 6$, colder walls are observed to trap more acoustic rays. In Fig. 5(c), the wall normal distance of the origin of the acoustic ray is varied for an adiabatic plate with $M_E = 6$. Fewer rays are trapped as the ray origin is translated from the surface. The results in Figs. 5(a), 5(b), and 5(c) do not change with Re_x because the flow field is assumed to be locally parallel and the boundary layer profiles are self-similar.

The non-parallel nature of the flow field can be included by interpolating the velocity and sound speed profiles calculated from the similarity solution for a certain range of Re_x and solving Eqs. 2. In Fig. 6, ray traces originating from the surface of an adiabatic flat plate with $M_E = 1$ and $\gamma = 7/5$ with an initial angle of inclination of $\theta_0 = 56, 57, 58$ are observed to bracket the value predicted in Fig. 5(a). The edge Mach number is increased to 6 for the rays in Fig. 7 and ray traces with an initial angle of inclination of $\theta_0 = 67, 68, 69$ bracket the maximum value predicted in Fig. 5(a). Changing the boundary condition at the wall to $T_W = T_{ad}/10$ should increase the maximum initial angle of inclination per Fig. 5(b). This is reflected in the rays with an initial angle of $\theta_0 = 82, 83, 84$.

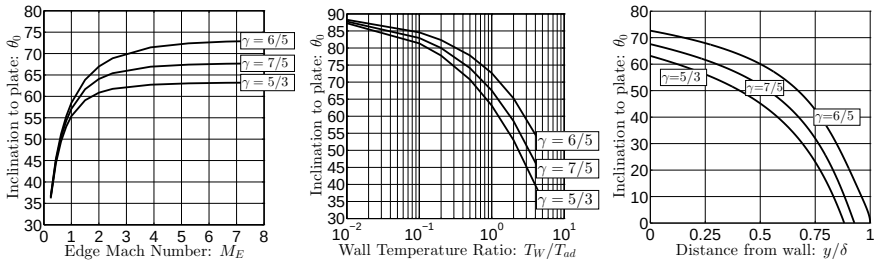

Fig. 5 a: Largest angle of inclination to the plate of acoustic ray that is refracted back to the surface, $M_E = 0.25 - 8$, $\gamma = 6/5, 7/5, 5/3$, $T_W = T_{ad}$. b: Largest angle of inclination to the plate of acoustic ray that is refracted back to the surface, $M_E = 6$, $\gamma = 6/5, 7/5, 5/3$, $T_W = KT_{ad}$, where K is varied between 10^{-2} and 5. c: Largest angle of inclination to the plate of acoustic ray that is refracted back to the surface at different wall normal origins, $M_E = 6$, $\gamma = 6/5, 7/5, 5/3$, $T_W = T_{ad}$.

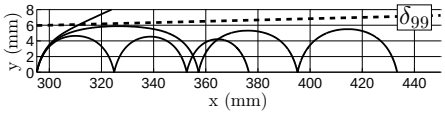

Fig. 6 Ray traces for $M_E = 1$, $\gamma = 7/5$, $T_W = T_{ad}$, with $\theta_0 = 56, 57, 58$ at $Re_{x0} = 1 \times 10^5$.

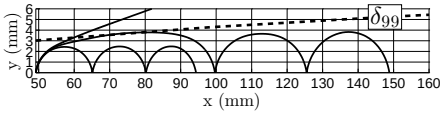

Fig. 7 Ray traces for $M_E = 6$, $\gamma = 7/5$, $T_W = T_{ad}$, with $\theta_0 = 67, 68, 69$ at $Re_{x0} = 1 \times 10^5$.

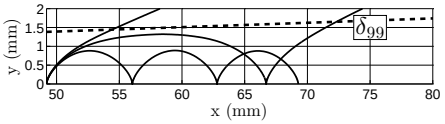

Fig. 8 Ray traces for $M_E = 6$, $\gamma = 7/5$, $T_W = T_{ad}/10$, with $\theta_0 = 82, 83, 84$ at $Re_{x0} = 1 \times 10^5$.

4 Conclusion

Ray-tracing in high-speed boundary layers has been used to explore the potential for acoustic energy trapping as function of edge Mach number, wall temperature ratio, and thermodynamic parameters. We proposed a figure of merit for acoustic energy trapping as the critical angle of inclination for rays originating in the boundary that are trapped, i.e., these rays always stay within the boundary layer. Using this concept, we find that an increasing amount of acoustic energy is trapped with increasing edge Mach number (M_E), and decreasing wall temperature ratio (T_W/T_{ad}). These trends agree qualitatively with the results of high-speed boundary layer stability calculation by Mack [1].

References

1. Mack, L. M., "Boundary-layer Linear Stability Theory," *AGARD Rep 709*, Special Course on Stability Transitional Laminar Flows 1984.
2. Pierce, A. D., *Acoustics: An Introduction to its Physical Principles and Applications*, Acoustical Society of America, Second ed., 1989.
3. Thompson, P. A., *Compressible-Fluid Dynamics*, McGraw-Hill, 1972.
4. G. A. Kriegsmann and E. L. Reiss, "Acoustic Propagation in Wall Shear Flows and the Formation of Caustics," *Journal of The Acoustical Society Of America*.
5. Goodman, R. R. and Duykers, L. R. B., "Calculations of Convergent Zones in a Sound Channel," *The Journal of the Acoustical Society of America*, Vol. 34, No. 7, 1962, pp. 960–962.
6. Munk, W. H., "Sound Channel in an Exponentially Stratified Ocean, with Application to SOFAR," *Journal of The Acoustical Society Of America*, Vol. 55, No. 2, 1974, pp. 220–226.
7. White, F., *Viscous Fluid Flow*, McGraw-Hill, 3rd ed., 2006.